SUPPORTING INFORMATION for Ionization of Nitric Acid on Crystalline Ice: the Role of Defects and Collective Proton Movement

S. Riikonen,[*,†] P. Parkkinen,[†] L. Halonen,[†] and R. B. Gerber[‡,¶,†]

Laboratory of Physical Chemistry, Department of Chemistry, University of Helsinki, P.O. Box 55, FI-00014, Helsinki, Finland, Institute of Chemistry and the Fritz Haber Research Center, The Hebrew University, Jerusalem 91904 Israel, and Department of Chemistry, University of California Irvine, Irvine, California 92697, United States

E-mail: sampsa.riikonen@iki.fi

Ice Surface Models

Figure 1 of the main article depicts the finite slab model used in the calculations. The slab has a vanishing dipole moment to the direction of the slab normal due to water molecule orientations that balance the net dipole moment. The surface dangling hydrogen bond arrangement corresponds to an order parameter[1] of 2, i.e., to a situation where the neighboring dangling bonds are far apart. This arrangement is known to be energetically favorable.[1,2] During geometry optimizations and molecular dynamics runs, movements of atoms were not constrained. Considering the topmost layer only, a single molecule adsorbed on this model slab corresponds to the coverage of ≈ 0.08

[*]To whom correspondence should be addressed

[†]Laboratory of Physical Chemistry, Department of Chemistry, University of Helsinki, P.O. Box 55, FI-00014, Helsinki, Finland

[‡]Institute of Chemistry and the Fritz Haber Research Center, The Hebrew University, Jerusalem 91904 Israel

[¶]Department of Chemistry, University of California Irvine, Irvine, California 92697, United States

ML. Using the definition of ML from Ref [3], namely, 4.6×10^{14} molecules/cm^2, a single adsorbed molecule in our model system corresponds to ≈ 0.1 ML.

Laboratory studies of ice grown on metal substrates indicate that, at low temperatures, the ice basal surface is full-bilayer terminated, while the topmost layer might be reconstructed and/or decorated (see Ref [4] and references therein). When increasing temperatures (180 - 260 K), surface premelting and the so-called quasi-liquid layer (QLL) steps in[4–7] making the surface gradually more liquid-like, starting from the topmost layers. In the present work, we are interested in temperature regimes T$\leq$200 K and also, from a fundamental point of view, in ice-like structures: crystalline surface structures similar to ours have earlier been used[8–11] to study ice surfaces.

Recently it has been realized that both the adsorption energies of water molecules[11] and defect formation energies[10] vary enormously on a crystalline ice surface. The adsorption energy can obtain, depending on the overall arrangement of the dangling OH bonds and the order parameter, values between $\sim$ 10 - 21 kcal/mol, [9,11] the high values corresponding to highly proton-ordered ice surfaces, while defect formations energies can vary between $\sim$ 5 - 21 kcal/mol. [10] This spread in adsorption and defect formation energies stems from the dipole-moment distribution of individual water monomers on an ice surface, which can be scattered.[10] Especially, the small defect formation energies and a defect "cascading" effect[10] contribute to surface roughness together with the monomer adsorption energies that can compete with surface energies.[9,11]

Some key energetics of the slab model, defect formation and adsorption energies are tabulated in Table S1. The water monomer adsorption energy into the "A2" site[9,11,12] is, in the present case, $\approx$30% larger than in earlier DFT calculations. We attribute this to the dispersion correction that has been included in our calculations. Same is true for the defect formation energies.

The stability of the slab model was tested by a 20 ps (picosecond) AIMD run at T=200 K and during this time the hexagonal structure was perfectly maintained. No water molecule rotations leading to different hydrogen bonding patterns than those of the original system took place.

Defect structures based on the slab model were constructed, as depicted in Figure 1 of the main article and in Figure S2: (AAD) or (ADD) species were removed from the topmost layer

and a local geometry optimization was performed, resulting in defects "LD_1" and "LD_2". In LD_1 a hydrogen bond between molecules (1) and (3) is formed while in LD_2, a weak hydrogen bond (as suggested by the O-H-O angle of $\sim 151°$) appears between molecules (2) and (4). "Annealed" defects (D_1 and D_2) were constructed by performing a few ps AIMD at T=200 K for LD_1 and LD_2. As suggested by Figure S2, LD_1 does not reconstruct during the AIMD, while LD_2 reconstructs slightly.

Table S1: Sublimation energy (E_{sub}) of the ice surface model (see Figure 1 of the main article), defect formation energies (E_{def}) for various defect structures (see Figure S2) and adsorption energies (E_{ads}) for nitric acid adsorption. Section "Optimization" gives values obtained from local geometry optimization: $H^+NO_3^-$ refers to spontaneous, while HNO_3 refers to non-dissociative adsorption. "MD" refers to molecular dynamics run: E_{ads} is obtained by performing a local relaxation at the end of the simulation (length of the simulation is indicated in parenthesis). "Meta-MD" refers to metadynamics and (E_{act}) to activation energy. Positive (negative) values indicate endothermic (exothermic) process. Our results are compared to earlier computational and experimental data in the rightmost part of the table. 1 kcal/mol = 4.184 kJ/mol.

Optimization		kcal/mol	Ref.		kcal/mol
P	E_{sub}	15.04			
LD_1	E_{def}	22.83	[10], Figure 2	E_{def}	4.6-20.8
LD_2	E_{def}	25.27			
D_2	E_{def}	22.57			
P^{H_2O} (A2-site)	E_{ads}	-17.91	[11] (DFT)	E_{ads}	-13.44
			[9] (DFT)		-12.73
			[12] (TIP4P)		-15.68
P^{HNO_3}		-22.54			
$LD_1^{H^+NO_3^-}$		-24.03			
$LD_2^{HNO_3}$		-24.46			
$D_2^{HNO_3}$		-19.89			
MD, T=200K					
$LD_2^{H^+NO_3^-}$	E_{ads} (7.7 ps)	-32.15			
$D_2^{H^+NO_3^-}$	E_{ads} (4.7 ps)	-27.92			
Meta-MD, T=200K					
$P^{H^+NO_3^-}$	E_{act}	4.62			
Reaction energies					kcal/mol
$E_{ads}(LD_2^{H^+NO_3^-})+E_{def}(LD_2)$	ΔE	-6.88	[13] (experimental)	ΔH	-12.91±0.62
			[14] (experimental)		-7.24±1.43
$E_{ads}(LD_2^{H^+NO_3^-})-E_{ads}(LD_2^{HNO_3})$		-7.69	[15], Table 8 (T=210 K)	ΔG	2.31-5.17
			[15], Table 8 (T=210 K)	ΔH	1.64-4.30

Computational Methods

The `CP2K/Quickstep` program package[16] with Density-functional theory (DFT), PBE generalized gradient (GGA) exchange- and correlation functional[17] (XCF) including Grimme's "D3" dispersion corrections[18] was used. The `Molopt` basis-set[19] was employed together with Goedecker-

Teter-Hutter[20] pseudopotentials. The surface slab model was decoupled from its periodic images using the Martyna-Tuckermann scheme,[21] with sufficient vacuum between the slab images. In all cases, if not otherwise stated, hydrogen was substituted with deuterium as this stabilizes the simulation and entitled us to use a larger timestep in time-integration, which we chose to be 0.75 fs (femtoseconds). All AIMD runs were performed in the NVT ensemble with the Nose-Hoover thermostat. In metadynamic[22] runs, scaling coefficient and the height of the Gaussians were 0.15 and 1.4×10^{-4} Hartree (1 Hartree = 2625.4996 kJ/mol), respectively. Gaussians were added at every 40 timesteps.

We have used the PBE XCF, which is known to give excellent results for ice.[23] In the context of DFT and proton transfer reactions, GGAs (typically BLYP) have been widely used.[24–26] On the other hand, it is recognized that all GGA XCFs underestimate the proton-transfer barrier[27–30] due to the self-interaction error. In detail, the barrier for proton transfer between two water molecules, as a function of their oxygen-oxygen distance d_{O-O}, falls to zero as d_{O-O} is reduced. The DFT method exaggerates this tendency, i.e., the barrier falls faster than with MP2 or coupled-cluster calculations, which may result in exaggerated rates for proton transfer reactions in AIMD simulations. Picosecond AIMD of (semi-)infinite systems with hybrid XC functionals is, in principle, possible[31] while computationally intensive and for this reason not considered in this work.

In Figure S1, the clusters and molecules that were calculated with two computational schemes, namely (1): PBE/`Molopt` scheme with dispersion corrections (DFT+D) and (2): Møller-Plesset second order perturbation theory[32] (MP2) as implemented in the TurboMole program.[33] Basis set used was `def2-TZVPD`.[34,35] Our MP2 results can be compared (for HNO_3 and MX), for example, to the B3LYP results of Ref [36]. Agreement in bond lengths is within $\sim$15 mÅ.

Bader occupational charges[37,38] for the test systems have been tabulated in Table S3, revealing a slightly higher electron population of protons in the DFT+D case. Sublimation energies for clusters M1 and MX using MP2 are -10.16 and -34.52 kcal/mol, while with DFT+D they are -10.97 and -38.55 kcal/mol, respectively. The DFT+D / `Molopt` then slightly overbinds ($\approx$ 0.7 kcal/mol per molecule) when compared to MP2 / `def2-TZVPD`.

Table S2: Bond lengths in Å as calculated with DFT+D and MP2 for nitric acid, nitrate ion and small clusters (MX, M1). See Figure S1.

	N(1)-O(1)	N(1)-O(2)	N(1)-O(3)	O(1)-H(1)	H(1)-O(4)	O(2)-H(3)	O(4)-H(2)	O(4)-H(3)	O(4)-H(6)	O(3)-H(4)	O(3)-H(5)
HNO_3 (DFT+D)	1.45	1.23	1.21	0.98							
(MP2)	1.40	1.21	1.20	0.98							
% err	3.21	1.16	0.92	0.82							
NO_3^-	1.28	1.28	1.28								
	1.26	1.26	1.26								
	1.59	1.51	1.51								
M1	1.40	1.24	1.22	1.02	1.69	2.18	0.97	0.98			
	1.37	1.22	1.20	1.00	1.70	2.41	0.97	0.97			
	2.41	1.64	1.00	1.80	-0.65	-9.71	0.83	1.24			
MX	1.37	1.24	1.23	1.06	1.51	1.94				2.17	2.20
	1.35	1.22	1.21	1.02	1.56	2.16				2.20	2.23
	1.56	1.72	1.24	3.13	-3.32	-10.12				-1.50	-1.21

Table S3: Bader occupational charges[37,38] from DFT+D and MP2 calculations in units of e^-. See Figure S1.

	N(1)	O(1)	O(2)	O(3)	O(4)	H(1)	H(2)	H(3)	H(4)	H(5)	H(6)
HNO_3 (DFT+D)	4.13	6.68	6.42	6.39		0.38					
(MP2)	4.07	6.72	6.43	6.41		0.36					
% err	1.47	-0.60	-0.16	-0.31		5.56					
NO_3^-	4.20	6.60	6.60	6.60							
	4.02	6.61	6.70	6.66							
	4.48	-0.15	-1.49	-0.90							
M1	4.17	6.66	6.46	6.38	7.59	0.38	0.38	0.35			
	4.04	6.72	6.48	6.46	7.26	0.33	0.34	0.32			
	3.22	-0.89	-0.31	-1.24	4.55	15.15	11.76	9.38			
MX	4.21	6.65	6.48	6.38	7.22	0.36		0.30	0.42	0.38	
	3.97	6.75	6.49	6.46	6.75	0.30		0.30	0.35	0.35	
	6.05	-1.48	-0.15	-1.24	6.96	20.0		1.56	20.0	8.57	

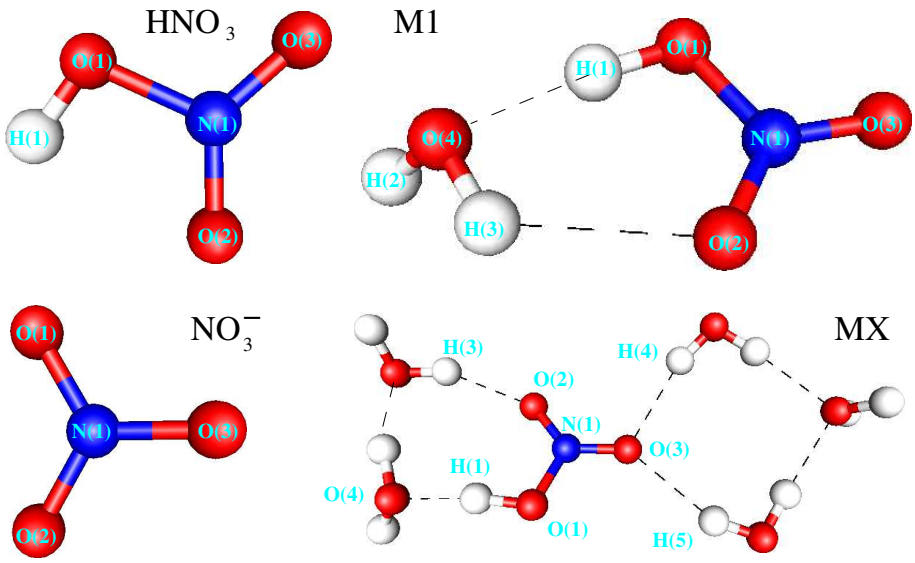

Figure S1: Molecules (nitric acid, nitrate) and small clusters (MX, M1) for test calculations (see Table S2 and Table S3).

Complementary Results

The main article describes in detail nitric acid ionization as it was adsorbed on defects LD_1 and LD_2 of Figure S2. Some AIMD snapshots from adsorption to annealed defect D_2 are depicted in Figure S3 and details are similar to the LD_2 case (see Figures 3-5 of the main article). However, in Figure S3 a stable CIP (contact ion pair) is formed before the collective proton jump and SSIP (solvent separater ion pair) formation.

Additionally, two cases where nitric acid was placed slightly ”off-site“ from the defect were studied. Figure S4 shows snapshots from one of them, in which the nitric acid proton was placed near molecule (M): during AIMD, nitric acid’s only hydrogen bond that was persistent throughout the simulation, was the one between acid’s proton and (M), while sporadic proton rattling events took place at this hydrogen bond. The defect then moved to the immediate vicinity of nitric acid, facilitating the ”presolvation“ of molecule (M) after 1.47 ps. The CIP did not occur, however, until 7.6 ps when the nitrate ion became solvated. In the final frame, a proton rattling event to the surface SSIP Eigen species takes place. The instantaneous CIP and SSIP events were correlated to situations where nitrate ion becomes temporarily solvated by four hydrogen bonds, however, nei-

ther a stable CIP or SSIP were formed during a 18 ps simulation as the nitrate ion has difficulties in finding a stable solvation structure (the hydrogen bond marked with an arrow was only temporarily available for the nitrate ion).

In yet another test case, nitric acid was placed in such a position that its proton formed a hydrogen bond with molecule (f) in Figure S4, i.e. even further from the defect site. In this case, the defect and nitric acid stayed separate during a 18 ps AIMD. No presolvation of (f) took place, while the binding state of nitric acid was again ”sloppy“; the only hydrogen bond that was persistent during the whole simulation, was the one between the acid's proton and (f).

The following conclusions from results presented in the main article and this Supporting Information can be drawn: (a) while a CIP and SSIP may form easily at defect sites, the rate limiting steps for ionization are the migration of defects and nitric acid itself. The defect and acid must find each other and furthermore, position accordingly in order to form a SSIP and (b) the persistent bond between the nitric acid proton and the surface molecule can lead, in picosecond timescales, to the ”presolvation“ of the molecule at the immediate vicinity of a defect. An atmospheric and ”rough“ ice surface has a high density of defects, admolecules and kinks that should facilitate these processes.

Once the SSIP formation is initiated, it's mechanism can be different to aqueous systems, as suggested by Figures 4 and 5 of the main article: a collective proton jump over two hydrogen bonds is observed, resulting directly in a SSIP and a proton residing in a surface Eigen site.

The SSIP formation on the pristine surface was studied using metadynamics. Details are given in Figure S5, where the free-energy is plotted as function of the first collective variable (first O-H bond length), for several values of the second collective variable (second O-H bond length). We associate most of the 4.62 kcal/mol reaction barrier to the fact that the acid is forcefully ionized, while the nitrate ion is not completely solvated (four hydrogen bonds are needed for complete solvation). On the other hand, the intermediate state where three protons jump simultaneously (J) is energetically close ($\leq$ 0.2 kcal/mol) to the final, solvent separated state. A collective proton jump involving three hydrogen bonds then seems likely, if the nitrate ion could be solvated by the

aid of, say, an admolecule or a kink site in an otherwise crystalline basal plane.

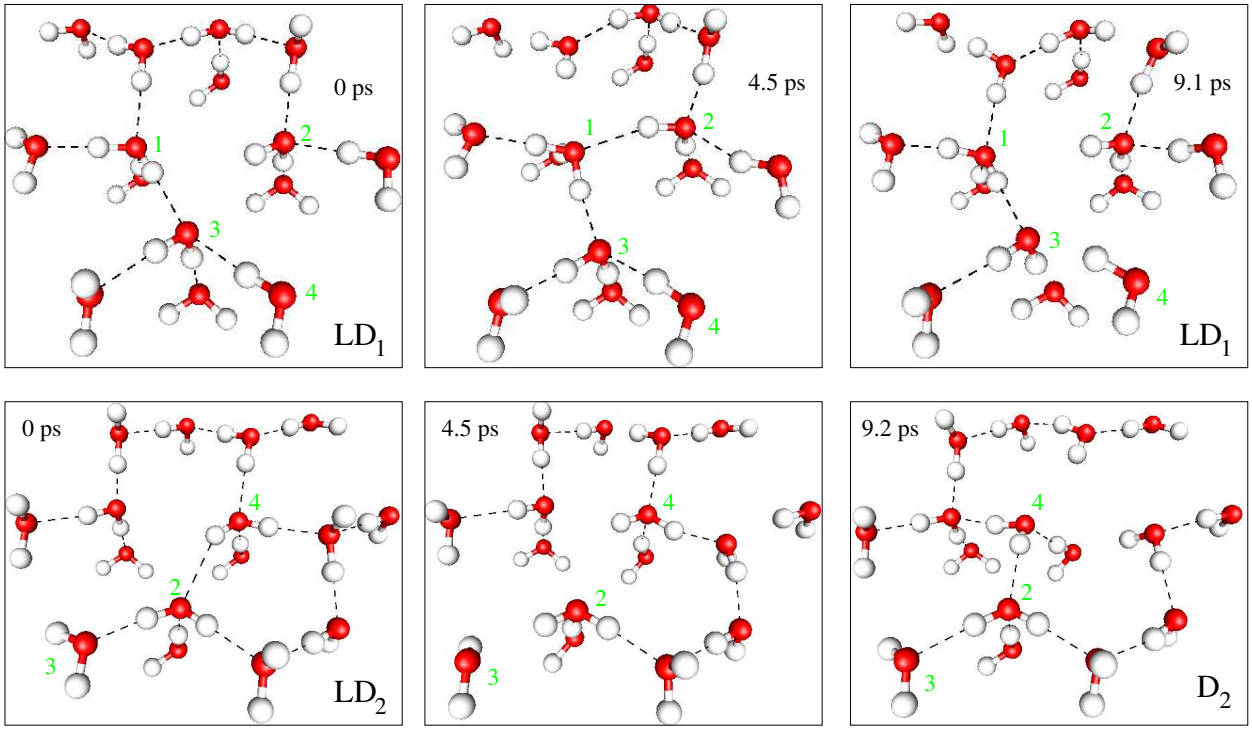

Figure S2: Snapshots of local structures of defects LD_1 (top row) and LD_2 (lowermost row) at T=200 K during $\approx$ 9 ps AIMD. Final geometries were stable during several picoseconds and they constitute the "annealed" defects LD_1 and D_2.

References

1. Pan, D.; Liu, L.-M.; Tribello, G. A.; Slater, B.; Michaelides, A.; Wang, E. Surface Energy and Surface Proton Order of the Ice Ih Basal and Prism surfaces. *Journal of Physics: Condensed Matter* **2010**, *22*, 074209.

2. Buch, V.; Groenzin, H.; Li, I.; Shultz, M. J.; Tosatti, E. Proton Order in the Ice Crystal Surface. *Proceedings of the National Academy of Sciences* **2008**, *105*, 5969–5974.

3. Marchand, P.; Marcotte, G.; Ayotte, P. Spectroscopic Study of HNO_3 Dissociation on Ice. *The Journal of Physical Chemistry A* **2012**, *116*, 12112–12122.

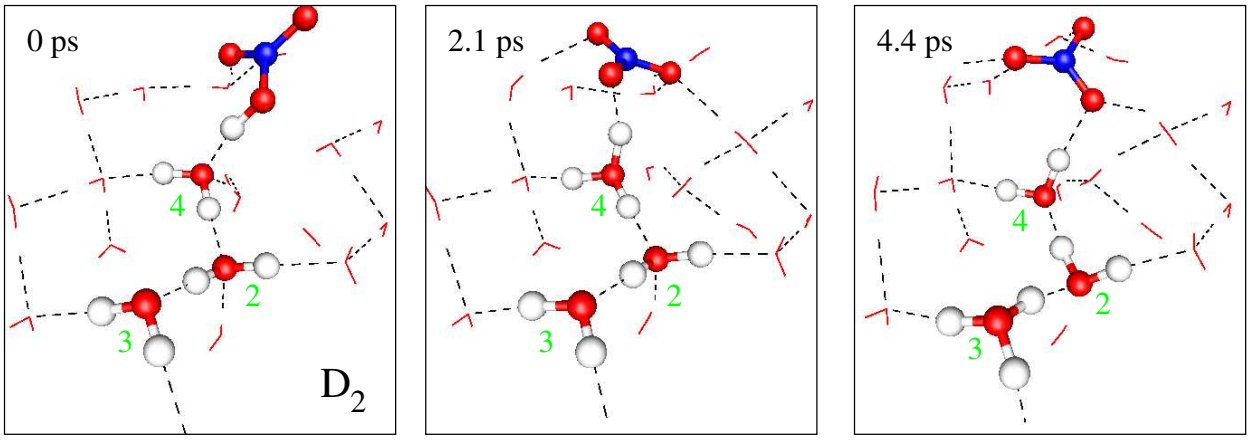

Figure S3: Snapshots of local structure of nitric acid adsorbed on defect D_2 during AIMD at T=200 K.

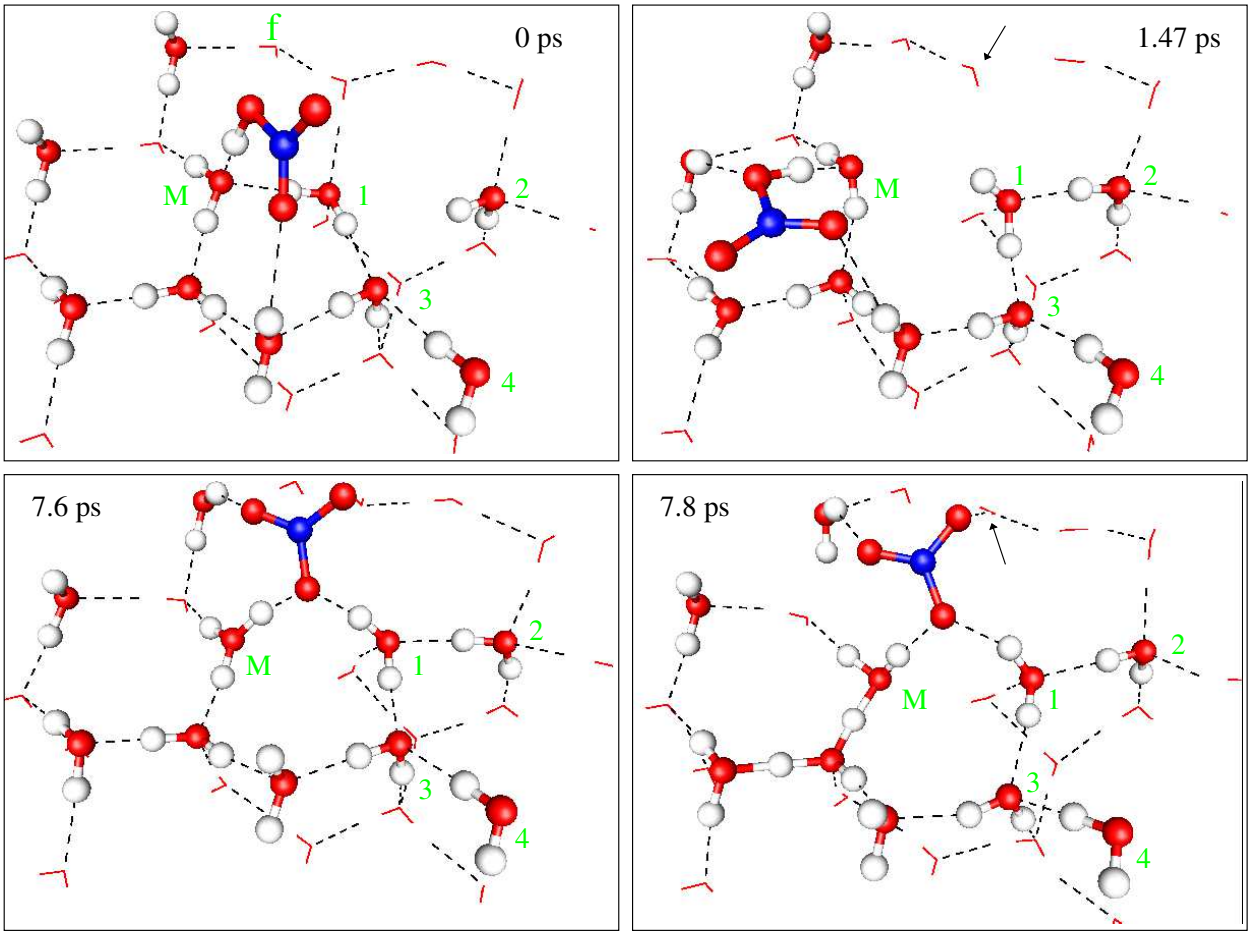

Figure S4: Snapshots of local structure of nitric acid adsorbed nearby defect LD_1 during AIMD at T=200 K.

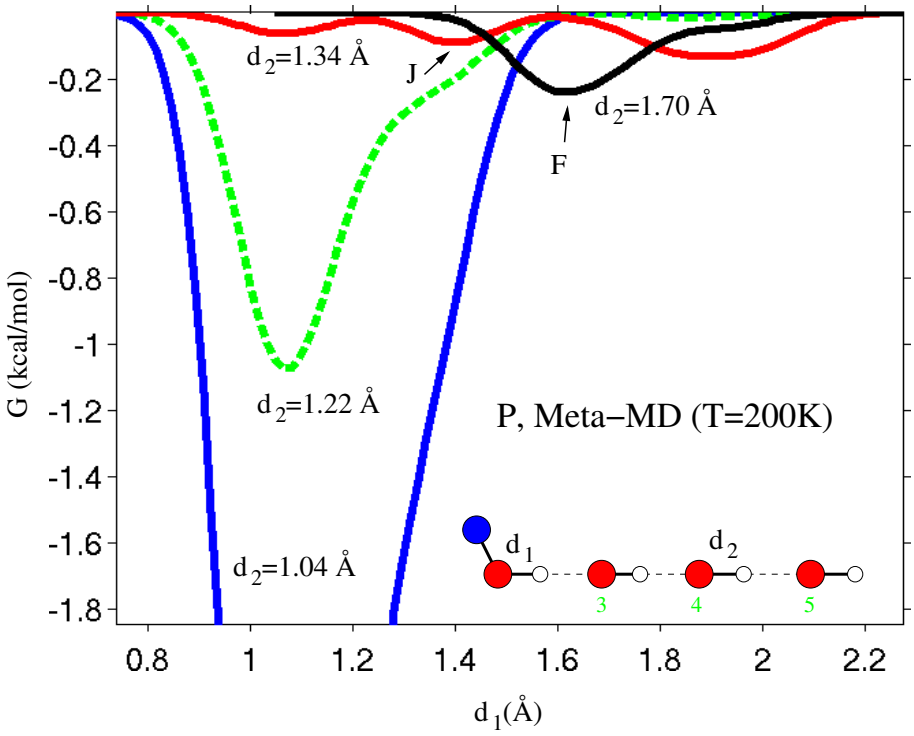

Figure S5: Free-energy surface from T=200 K metadynamics run for system (P) (see also Figure 3(a) of the main article). Collective variables are two OH bondlengths (d_1 and d_2, see the inset), which are used to enforce the proton relay. An intermediate state where both protons relay simultaneously is indicated (J), together with the final state (F). Oxygen (red spheres) and hydrogen (white spheres) atoms are indicated and enumerated in the inset. Each curve corresponds to a distinct value of d_2.

4. Park, S.-C.; Moon, E.-S.; Kang, H. Some Fundamental Properties and Reactions of Ice Surfaces at Low Temperatures. *Phys. Chem. Chem. Phys.* **2010**, *12*, 12000–12011.

5. Huthwelker, T.; Ammann, M.; Peter, T. The Uptake of Acidic Gases on Ice. *Chemical Reviews* **2006**, *106*, 1375–1444.

6. Mundy, C. J.; Kuo, I.-F. W. First-Principles Approaches to the Structure and Reactivity of Atmospherically Relevant Aqueous Interfaces. *Chemical Reviews* **2006**, *106*, 1282–1304.

7. Mantz, Y. A.; Geiger, F. M.; Molina, L. T.; Molina, M. J.; Trout, B. L. First-principles Molecular-dynamics Study of Surface Disordering of the (0001) Face of Hexagonal Ice. *The Journal of Chemical Physics* **2000**, *113*, 10733–10743.

8. Mantz, Y. A.; Geiger, F. M.; Molina, L. T.; Molina, M. J.; Trout, B. L. The interaction of HCl with the (0001) face of hexagonal ice studied theoretically via Car–Parrinello molecular dynamics. *Chemical Physics Letters* **2001**, *348*, 285 – 292.

9. Thierfelder, C.; Hermann, A.; Schwerdtfeger, P.; Schmidt, W. G. Strongly Bonded Water Monomers on the Ice Ih Basal Plane: Density-Functional Calculations. *Phys. Rev. B* **2006**, *74*, 045422.

10. Watkins, M.; Pan, D.; Wang, E. G.; Michaelides, A.; VandeVondele, J.; Slater, B. Large Variation of Vacancy Formation Energies in the Surface of Crystalline Ice. *Nat Mater* **2011**, *10*, 794–798.

11. Sun, Z.; Pan, D.; Xu, L.; Wang, E. Role of Proton Ordering in Adsorption Preference of Polar Molecule on Ice Surface. *Proceedings of the National Academy of Sciences* **2012**, *109*, 13177–13181.

12. Batista, E. R.; Jónsson, H. Diffusion and Island formation on the ice Ih basal plane surface. *Computational Materials Science* **2001**, *20*, 325 – 336, 9th Int. Workshop on Computational Materials Science.

13. Hynes, R. G.; Fernandez, M. A.; Cox, R. A. Uptake of HNO_3 on Water-ice and Coadsorption of HNO_3 and HCl in the Temperature Range 210–235 K. *Journal of Geophysical Research: Atmospheres* **2002**, *107*, AAC 19–1–AAC 19–11.

14. Ullerstam, M.; Thornberry, T.; Abbatt, J. P. D. Uptake of Gas-phase Nitric Acid to Ice at Low Partial Pressures: Evidence for Unsaturated Surface Coverage. *Faraday Discuss.* **2005**, *130*, 211–226.

15. Bianco, R.; Wang, S.; Hynes, J. T. Theoretical Study of the Dissociation of Nitric Acid at a Model Aqueous Surface. *The Journal of Physical Chemistry A* **2007**, *111*, 11033–11042.

16. VandeVondele, J.; Krack, M.; Mohamed, F.; Parrinello, M.; Chassaing, T.; Hutter, J. Quickstep: Fast and Accurate Density Functional Calculations Using a Mixed Gaussian and Plane Waves Approach. *Computer Physics Communications* **2005**, *167*, 103 – 128.

17. Perdew, J. P.; Burke, K.; Ernzerhof, M. Generalized Gradient Approximation Made Simple. *Phys. Rev. Lett.* **1996**, *77*, 3865–3868.

18. Grimme, S.; Antony, J.; Ehrlich, S.; Krieg, H. A Consistent and Accurate *ab initio* Parametrization of Density Functional Dispersion Correction (DFT-D) for the 94 Elements H-Pu. *The Journal of Chemical Physics* **2010**, *132*, 154104.

19. VandeVondele, J.; Hutter, J. Gaussian Basis Sets for Accurate Calculations on Molecular Systems in Gas and Condensed Phases. *The Journal of Chemical Physics* **2007**, *127*, 114105.

20. Goedecker, S.; Teter, M.; Hutter, J. Separable Dual-space Gaussian Pseudopotentials. *Phys. Rev. B* **1996**, *54*, 1703–1710.

21. Martyna, G. J.; Tuckerman, M. E. A Reciprocal Space Based Method for Treating Long Range Interactions in *ab initio* and Force-field-based Calculations in Clusters. *The Journal of Chemical Physics* **1999**, *110*, 2810–2821.

22. Laio, A.; Parrinello, M. Escaping Free-energy Minima. *Proceedings of the National Academy of Sciences* **2002**, *99*, 12562–12566.

23. Hamann, D. R. H_2O Hydrogen Bonding in Density-Functional Theory. *Phys. Rev. B* **1997**, *55*, R10157–R10160.

24. Marx, D.; Tuckerman, M. E.; Hutter, J.; Parrinello, M. The Nature of the Hydrated Excess Proton in Water. *Nature* **1999**, *397*, 601–604.

25. Marx, D. Proton Transfer 200 Years after von Grotthuss: Insights from *Ab Initio* Simulations. *ChemPhysChem* **2006**, *7*, 1848–1870.

26. Kulig, W.; Agmon, N. A 'Clusters-in-liquid' Method for Calculating Infrared Spectra Identifies the Proton-transfer Mode in Acidic Aqueous Solutions. *Nat Chem* **2013**, *5*, 29–35.

27. Mijoule, C.; Latajka, Z.; Borgis, D. Density Functional Theory Applied to Proton-transfer Systems. A Numerical Test. *Chemical Physics Letters* **1993**, *208*, 364 – 368.

28. Barone, V.; Orlandini, L.; Adamo, C. Proton Transfer in Model Hydrogen-bonded Systems by a Density Functional Approach. *Chemical Physics Letters* **1994**, *231*, 295 – 300.

29. Sadhukhan, S.; Muñoz, D.; Adamo, C.; Scuseria, G. E. Predicting Proton Transfer Barriers with Density Functional Methods. *Chemical Physics Letters* **1999**, *306*, 83 – 87.

30. Nachimuthu, S.; Gao, J.; Truhlar, D. G. A Benchmark Test Suite for Proton Transfer Energies and Its Use to Test Electronic Structure Model Chemistries. *Chemical Physics* **2012**, *400*, 8 – 12.

31. Guidon, M.; Hutter, J.; VandeVondele, J. Robust Periodic Hartree-Fock Exchange for Large-Scale Simulations Using Gaussian Basis Sets. *Journal of Chemical Theory and Computation* **2009**, *5*, 3010–3021.

32. Møller, C.; Plesset, M. S. Note on an Approximation Treatment for Many-Electron Systems. *Phys. Rev.* **1934**, *46*, 618–622.

33. TURBOMOLE V6.4 2012, a development of University of Karlsruhe and Forschungszentrum Karlsruhe GmbH, 1989-2007, TURBOMOLE GmbH, since 2007; available from `http://www.turbomole.com`.

34. Weigend, F.; Ahlrichs, R. Balanced Basis Sets of Split Valence, Triple Zeta Valence and Quadruple Zeta Valence Quality for H to Rn: Design and Assessment of Accuracy. *Phys. Chem. Chem. Phys.* **2005**, *7*, 3297–3305.

35. Rappoport, D.; Furche, F. Property-optimized Gaussian Basis Sets for Molecular Response Calculations. *The Journal of Chemical Physics* **2010**, *133*, 134105.

36. Gonzalez, J.; Anglada, J. M. Gas Phase Reaction of Nitric Acid with Hydroxyl Radical without and with Water. A Theoretical Investigation. *The Journal of Physical Chemistry A* **2010**, *114*, 9151–9162.

37. Bader, R. *Atoms in Molecules: A Quantum Theory*; Oxford University Press USA (1994).

38. Tang, W.; Sanville, E.; Henkelman, G. A Grid-based Bader Analysis Algorithm Without Lattice Bias. *Journal of Physics: Condensed Matter* **2009**, *21*, 084204.